Magnetotransport as a probe of phase transformations in metallic antiferromagnets: The case of $UIrSi_3$

F. Honda,[1] J. Valenta,[2] J. Prokleška,[2] J. Pospíšil,[2] P. Proschek,[2] J. Prchal,[2] and V. Sechovský[2]
[1]*Tohoku University, Institute for Materials Research, Narita-cho 2145-2, Oarai, Ibaraki, Japan*
[2]*Charles University, Faculty of Mathematics and Physics, Department of Condensed Matter Physics, Ke Karlovu 5, Prague 2, Czech Republic*

(Received 2 December 2018; revised manuscript received 9 June 2019; published 1 July 2019)

The electrical resistance, Hall resistance, and thermoelectric power of the Ising-like antiferromagnet $UIrSi_3$ were measured as functions of temperature and magnetic field. We have observed that the unequivocally different characters of first-order and second-order magnetic phase transitions lead to distinctly different magnetotransport properties in the neighborhood of corresponding critical temperatures and magnetic fields, respectively. The magnetic contributions to the electrical and Hall resistivity in the antiferromagnetic state, and the polarized and normal regimes of paramagnetic state are driven by different underlying mechanisms. Results of detailed measurements of magnetotransport in the vicinity of the tricritical point reveal that the Hall-resistivity steps at phase transitions change polarity just at this point. The jumps in field dependences of specific heat, electrical resistivity, Hall resistivity, and Seebeck coefficient at the first-order metamagnetic transitions indicate a Fermi surface reconstruction, which is characteristic of a magnetic-field-induced Lifshitz transition. The presented results emphasize the usefulness of measurements of electrical- and thermal-transport properties as sensitive probes of magnetic phase transformations in antiferromagnets sometimes hardly detectable by other methods.

DOI: 10.1103/PhysRevB.100.014401

I. INTRODUCTION

Since the electrical transport can be influenced by interactions of conduction electrons with magnetic fields and with unpaired electrons carrying magnetic moments, the electrical resistivity and Hall resistivity may serve as important probes of the details of magnetism in metallic materials.

The electrical resistivity ρ in magnetic metals is considered within a simple approach, supposing validity of Mathiessens' rule, as a sum:

$$\rho = \rho_0 + \rho_{\text{e-p}} + \rho_{\text{mag}}. \quad (1)$$

The temperature independent residual-resistivity term ρ_0, which originates in the scattering of conduction electrons from lattice defects, and the electron-phonon term $\rho_{\text{e-p}}$ reflecting the scattering of conduction electrons from phonons are present in all metallic materials. The latter term represents the scattering of conduction electrons from magnetic moments due to exchange interaction with unpaired electrons carrying the moment.

The states of $5f$ electrons carrying magnetic moments in uranium intermetallics can form a narrow band at the Fermi level. The strong interaction with conduction electron states causes significantly enhanced scattering of conduction electrons from U magnetic moments. The ρ_{mag} values of U intermetallics in a paramagnetic (PM) state are usually high and roughly temperature independent. At temperatures below the magnetic-ordering temperature, ρ_{mag} decreases with temperature in a characteristic way for magnetic excitations, especially magnons [1,2].

In ferromagnets, ρ_{mag} vanishes in the low temperature limit. On the other hand, rather large ρ_{mag} values are usually observed for antiferromagnetic (AFM) U materials even at the lowest temperatures. Resistance measurements on anisotropic materials reveal the anomalously large ρ_{mag} low-temperature values for the current applied along the directions with AFM coupling of magnetic moments [3,4].

The uranium-based antiferromagnets with uniaxial anisotropy [3,5–8] exhibit magnetic behavior such as the Ising antiferromagnets [9,10]. These strongly anisotropic antiferromagnets are generally characterized by simple reversals of the local magnetic moment directions. When cooled in zero field, they undergo a second-order magnetic phase transition (SOMPT) from a PM to an AFM state at T_{N}. Below T_{N}, they are ordered antiferromagnetically with a sublattice structure, in which the large anisotropy constrains the magnetic moments to point either parallel or antiparallel to the easy axis. On the application of a magnetic field along the easy axis a metamagnetic transition (MT) from the AFM to the PM state takes place at a critical field H_{c}. At sufficiently low temperatures, MT is a first-order magnetic phase transition (FOMPT) characterized by a sudden reversal of antiparallel sublattices to the direction of the applied field. The high-field ($H > H_{\text{c}}$) state is characterized by ferromagnetic-like aligned magnetic moments but it is a paramagnetic (not ferromagnetic) state [11]. Due to its character it is called a field polarized paramagnet (PPM) regime [12,13].

The first-order metamagnetic transition between the AFM state and the PPM regime in uranium-based antiferromagnets with uniaxial anisotropy is accompanied by a dramatic drop of electrical resistivity [3,5–8,14,15] and ρ_{mag} practically vanishes in the low-temperature limit similar to ρ_{mag} in ferromagnets. The negative magnetoresistance jumps observed at H_{c} on uranium-based antiferromagnets [3,5–8,14,15] quantitatively

compare to the giant magnetoresistance (GMR) reported in magnetic multilayers [16].

The large low-temperature resistivity and negative magnetoresistance values, respectively, in antiferromagnets have generally two underlying mechanisms. When the AFM periodicity does not coincide with the crystallographic (chemical) unit cell, a reconstruction of the Fermi surface (FS) may occur at the transition temperature, assuming that a new Brillouin zone boundary cuts the FS. As a result, an electron energy gap may be created along the new periodicity direction. This leads to a reduction in the effective number of charge carriers and a consequent increase of resistivity. This approach has been used as an explanation of the ρ increase in AFM lanthanide compounds below T_N [17]. On the other hand, the AFM periodicity is removed by the MT from AFM to PPM, so the AFM gaps in the FS are consequently closed and the electrical conductivity is correspondingly recovered.

The major portion of the giant negative magnetoresistance observed at the MT in the Ising-like uranium antiferromagnets cannot be explained by the mechanism based on a FS gapping. The spin-dependent scattering mechanism involving mainly the scattering due to $\uparrow\downarrow$ coupled U magnetic moments in the AFM structure [4] may be considered as dominant. This concept is analogous to the approach to GMR in magnetic multilayers [16,18,19]. Within a certain interval of temperatures below T_N the MT is a continuous transition (SOMPT). The applied magnetic field ($H < H_c$) along the easy axis induces fluctuations from an AFM state. These fluctuations are multiplying with increasing magnetic field up to H_c. The conduction electrons scatter from the fluctuations that lead to progressively increasing ρ_{mag} [20]. At H_c, a peak in the $\rho_{mag}(T)$ dependence has been found by calculations [21] and experiment, e.g., on V_5S_8 [22].

The line of critical points of the SOMPTs at high temperatures and the line of critical point of the FOMPTs at low temperatures meet at a point that is known as the tricritical point (TCP). No systematic magnetotransport data on anisotropic U antiferromagnets involving SOMPTs and their evolution in the vicinity of a TCP have been reported so far, to our knowledge.

The ordinary Hall effect arising from the Lorentz force acting on the charge carriers turned out to be a useful tool for determination of charge-carrier density in nonmagnetic materials and played an important role in the early years of semiconductor physics research as well as related solid-state electronics. The normal Hall resistivity provides, for single-band metals, a measure of the volume in momentum space enclosed by the FS. In materials possessing magnetization an additional contribution comes into play as a consequence of the anomalous Hall effect (AHE). The total Hall resistivity can be described empirically as a sum of two terms; the normal and the anomalous Hall resistivity [23–27]:

$$\rho_H(H) = R_H \mu_0 H = R_o \mu_0 H + R_s M, \tag{2}$$

where R_o and R_s are the normal and the anomalous Hall coefficient, respectively, H is the applied magnetic field and M is the volume magnetization both perpendicular to the plane in which the Hall resistivity is measured. Thus the single Hall coefficient is written as:

$$R_H = R_o + R_s \frac{M}{\mu_0 H}. \tag{3}$$

An AHE is caused by three underlying mechanisms; the first one is intrinsically caused by specific features of band structure (Berry phase), the other two involve the left-right asymmetric scattering due to the skew scattering and the side-jump scattering of conduction electrons. The anomalous Hall coefficient can be expressed as a sum of two terms:

$$R_s = a\rho + b\rho^2, \tag{4}$$

where $a\rho$ represents the skew-scattering and $b\rho^2$ the intrinsic and side-scattering mechanisms. The AHE has been in fact recognized on ferromagnetic iron already by Hall [28]. Pugh and Lippert [23,24] have shown that the empirical formula (2) applies to many materials over a broad range of external magnetic fields. In ferromagnets, the second term represents the contribution due to the spontaneous magnetization [23–26]. The studies on the Hall effect in antiferromagnets have a much shorter history than the research in the AHE in ferromagnets. Recently, much interest has arisen in the AHE in noncollinear transition-metal antiferromagnets, in which a sizable AHE can be found also in the state with zero net magnetization [29–32]. These materials offer promising opportunities in topological antiferromagnetic spintronics [33].

The Hall effect was investigated in several antiferromagnetic f-electron intermetallics during periods ofresearch interest in fluctuating-valence, Kondo-lattice and heavy-fermion lanthanide [34–39], and uranium compounds [40–44]. Several papers were dedicated to the investigation of the Hall effect related to metamagnetic transitions in AFM materials [45–50].

This paper is devoted to a detailed investigation of magnetotransport properties of $UIrSi_3$ in relation with its specific magnetism. It is one of the only two known uranium intermetallic compounds adopting the noncentrosymmetric tetragonal $BaNiSn_3$-type structure. Antiferromagnetism of $UIrSi_3$ at temperatures below 42 K was reported by Buffat *et al.* [51] from experiments on polycrystals. They also observed a metamagnetic-like transition in $\mu_0 H = 5.6$ and 3.2 T at $T = 30$ and 38 K, respectively.

Recently, $UIrSi_3$ single crystals have been grown and subjected to magnetization and specific-heat measurements [6]. The antiferromagnetism below the Néel temperature $T_N = 41.7$ K has been confirmed. Magnetization and specific-heat data revealed a strong uniaxial anisotropy in the AFM state with the c axis, as the easy magnetization direction places $UIrSi_3$ among the Ising systems. When a magnetic field is applied along the c axis it undergoes a MT from the AFM to a PM state at a critical field H_c. No MT is observed when the field is applied along the a axis, up to 14 T.

At temperatures below 28 K, the MT is a FOMPT ($\mu_0 H_c = 7.3$ T at 2 K) to a PPM regime. The saturated magnetization in the PPM regime amounts to $0.66\,\mu_B$/f.u. This value is rather small in comparison to the expected values of the U^{3+} and U^{4+} free-ion ordered moments, 3.20 and $3.27\,\mu_B$, respectively, which suggests an itinerant character of the $5f$-electron magnetism (if Ir and Si magnetic moments can be neglected).

A second-order metamagnetic transition is observed at higher temperatures ($28\text{K} > T > T_N$). The point in the H-T magnetic phase diagram where the transition switches between a FOMPT and a SOMPT is considered as the tricritical point (at $T_{tcp} = 28$ K and $\mu_0 H_{tcp} = 5.8$ T).

The main objective of this work is to determine the manifestation of various magnetic phase transitions in the Ising itinerant $5f$-electron antiferromagnet $UIrSi_3$ in magnetotransport properties. For this purpose numerous isofield $\rho_{[001]}(T)$,$\rho_{[100]}(T)$, $\rho_H(T)$ and isothermal $\rho_{[001]}(H)$,$\rho_{[100]}(H)$, $\rho_H(H)$ dependences were measured within wide intervals of temperatures (2–300 K) and fields (0–14 T) parallel to the easy-magnetization direction, i.e., the c axis. To assure the best quality of samples a new $UIrSi_3$ single crystal has been grown employing our experience from previous work [6].

All three resistivities were found to be sensitive to magnetic-phase transitions in $UIrSi_3$. The $\rho(T)$ and $\rho_H(T)$ dependences measured in various magnetic fields exhibit considerable anomalies at corresponding critical temperatures $T_N(H)$. The $\rho(H)$ and $\rho_H(H)$ isotherms show anomalies at corresponding critical fields of MT, $H_c(T)$. The $T_N(H)$ and $H_c(T)$ values fit very well with the magnetic phase diagram [6] derived using magnetization and specific-heat measurements. The character of the anomalies corresponding to FOMPTs and SOMPTs has been found to be strikingly different. The observed change of polarity of the $\Delta\rho_H(T)$ and $\Delta\rho_H(H)$ steps at the temperature and magnetic field where the FOMPT changes to a SOMPT may offer a useful criterion for determination of the TCP in Ising antiferromagnets.

We have also measured the thermoelectric effect at several temperatures as a function of magnetic field. The drop of the value of the Seebeck coefficient observed at the H_c of the FOMPT in conjunction with the corresponding jumps in $\rho(H)$, $\rho_H(H)$, and $C_p(H)$ dependences provide strong indications that the FOMPT in $UIrSi_3$ is probably a Lifshitz transition, which is characterized by a FS reconstruction.

II. EXPERIMENTAL

A $UIrSi_3$ single crystal has been prepared by the floating zone melting method in a commercial four-mirror optical furnace with halogen lamps, each 1 kW (model FZ-T-4000-VPM-PC, Crystal Systems Corp., Japan). In the first step, a polycrystalline material of $UIrSi_3$ was synthesized by arc-melting from stoichiometric amounts of the pure elements U (3N, further treated by Solid State Electrotransport [52,53]), Ir (4N), and Si (6N) in an Ar (6N) protective atmosphere. No sign of evaporation was detected during the melting. Then, a precursor in the form of a 50-mm long rod was prepared by arc melting in a special water-cooled copper mold at identical protective conditions. The quartz chamber of the optical furnace was evacuated by a turbomolecular pump to 10^{-6} mbar before the crystal growth process. In order to desorb gases from the surface of the precursor, the power of the furnace was increased gradually up to 30% of maximum power (far below the melting at ∼54% power) and the precursor was passed through the hot zone several times while continuously evacuating. After the degas process and evacuation, the quartz chamber was quickly filled with high purity Ar (6N). The whole growth process was performed with

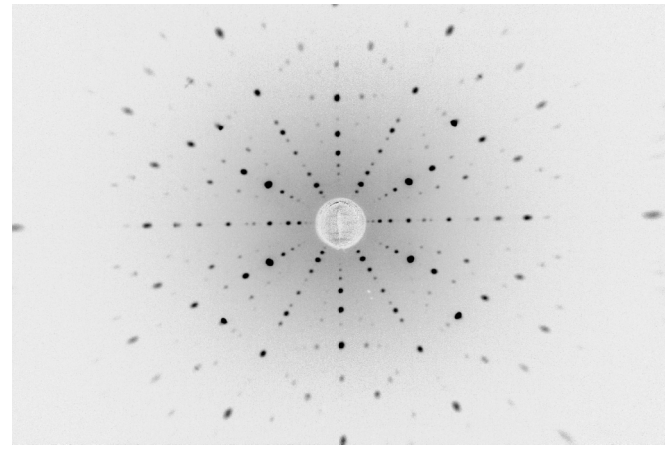

FIG. 1. Laue pattern of the $UIrSi_3$ single crystal oriented along [110].

Ar flow of 0.25 l/min and a pressure of ∼2 bar. A narrow neck was created in the beginning of the growth process by variation of the speed of the upper and bottom pulling shafts. The pulling rate was very slow, only 0.5 mm/h, and without rotation. A large single crystal of a cylindrical shape with length ∼50 mm and diameter 4 mm was obtained. The high quality and orientation of the single crystal was verified by the Laue method (Fig. 1). The stoichiometric composition was verified by a scanning electron microscopy using a Tescan Mira I LMH system equipped with an energy-dispersive x-ray detector Bruker AXS. The analysis revealed a single phase single crystal of 1:1:3 composition. Detailed surface analysis did not detect any foreign phases.

The characterization of this crystal has been done by magnetization and specific-heat measurements analogous to these reported in Ref. [6]. The obtained results were in fair agreement with data presented before [6].

All data presented in this paper have been measured in magnetic fields applied exclusively along the c axis of the tetragonal structure of $UIrSi_3$. The electrical resistivity, Hall resistivity, thermoelectric power, magnetization, and specific heat were measured with a physical property measurement system (PPMS, Quantum Design Inc.) in fields up to 14 T. For determination of T_N from the temperature dependence of the specific heat, the point of the balance of entropy released at the phase transition method was used. The specific heat was measured on a basal-plane plate sample of 11 mg mass. Resistivity measurements were performed on two bar-shaped samples ($1.8 \times 0.75 \times 0.73\,\text{mm}^3$ and $1.1 \times 0.78 \times 0.55\,\text{mm}^3$ for current applied along the a and c axis, respectively). The Hall resistivity was measured with a basal-plane plate sample (diameter of 1.2 mm) with current applied along the a axis and the Hall voltage measured in the perpendicular direction in the basal plane. The sample for thermoelectric power measurements was a $1 \times 1 \times 4\,\text{mm}^3$ c-axis bar.

The field dependences of electrical resistivity $\rho(H)$, Hall resistivity $\rho_H(H)$, thermoelectric power $S(H)$ and magnetization $M(H)$ were measured in fields between 4 and 8 T at a sweep rate of 1, 2.5, 2.5, and 2 mT/s, respectively. The system has been found to be only slightly relaxing. A typical time dependence of electrical resistance at a most "sensitive"

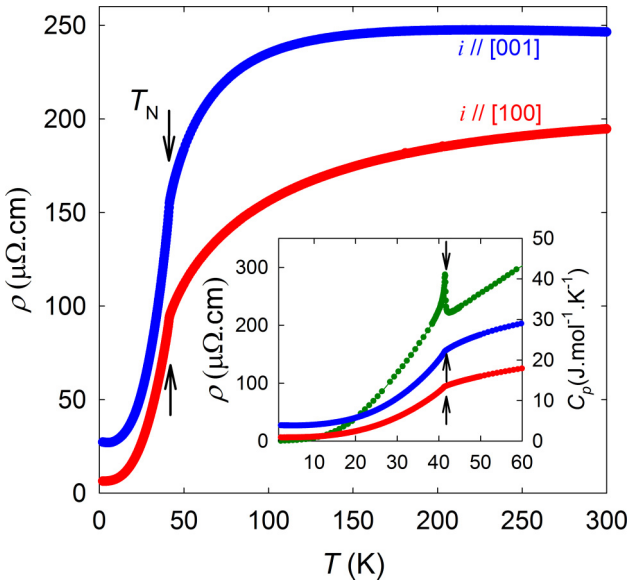

FIG. 2. Temperature dependence of the electrical resistivity of $UIrSi_3$ for electrical current parallel to the [100] and [001] direction, respectively. Inset: a low-temperature detail including also the corresponding specific-heat C_p vs T (green points) plot. The arrows marks T_N.

point of the hysteresis loop (see Fig. S1 in the Supplemental Material [54]) is seen in Fig. S2. This demonstrates that the hysteresis of the FOMPT observed in $\rho(H)$, $\rho_H(H)$, $S(H)$, and $M(H)$ is intrinsic and not an artefact of fast sweeping the applied magnetic field.

III. RESULTS AND DISCUSSION

The observed anisotropy of the temperature dependence of the electrical resistivity, $\rho(T)$ (see Fig. 2) indicates an anisotropic FS of $UIrSi_3$. The resistivities $\rho_{[100]}(T)$ and $\rho_{[001]}(T)$ for current i // [100] and [001], respectively, increase with increasing temperature above T_N and gradually saturate [the curvature and tendency to saturation is more pronounced in the $\rho_{[001]}(T)$ dependence]. This resembles the behavior of transition metals and their compounds characterized by a narrow d-electron band crossing the Fermi level (E_F), which was explained by an s-d scattering mechanism as proposed by Mott [55] and Jones [56]. We tentatively suppose that the resistivity of U intermetallics characterized by a narrow $5f$-electron band crossing the E_F could be considered within an analogous s-f scattering model.

The negative curvature of both, $\rho_{[100]}(T)$ and $\rho_{[001]}(T)$ observed at high temperatures suddenly changes to a convex dependence at the same characteristic temperature, which coincides with the T_N value determined from specific-heat data (see inset of Fig. 2). The RRR values are 34 and 14, respectively.

When we apply the magnetic field along the [001] direction the T_N-related anomaly in the $\rho_{[100]}(T)$ and $\rho_{[001]}(T)$ dependences are shifted to lower temperatures with increasing field such that they follow the corresponding specific-heat anomaly (see Fig. 3). The resistivity anomaly at T_N simultaneously develops with increasing the field from a just-negative $\partial\rho/\partial T$

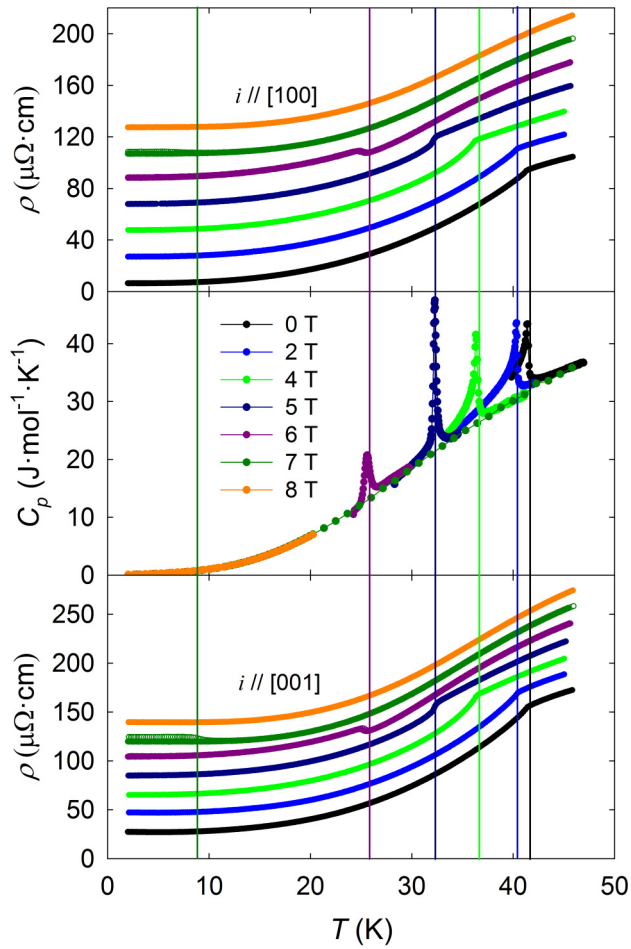

FIG. 3. Temperature dependences of the electrical resistivity for the current parallel to the [100] and [001] directions (top and bottom panel, respectively) and specific heat (middle panel) of $UIrSi_3$ below 45 K in the magnetic field applied in the [001] direction. The ρ vs T curves measured in different fields are mutually shifted by 20 μΩ cm along the vertical axis for clarity. The actual vertical scale corresponds to the 0-T curve. The colored vertical lines represent the T_N values corresponding to the actual applied magnetic fields. The 7-T line corresponds to the bifurcation point of the FC and ZFC resistivity curves.

change in zero field to a clear positive $\Delta\rho$ step in 5 T for the AFM to PM transition. T_N is associated with the maximum of $\partial\rho/\partial T$. In 6 T we suddenly observe a negative $\Delta\rho$ step at T_N for the AFM to PPM transition, which is evidenced also by the zero-field-cooled (ZFC) curves measured in 7 T. The 8-T $\rho_{[100]}(T)$ and $\rho_{[001]}(T)$ curves are smooth showing no sharp anomaly within the entire temperature range. A detailed view of the evolution of $\rho_{[001]}(T)$ curves in fields from 5 to 8 T is displayed in Fig. 4. The corresponding magnetization $M(T)$ dependences shown in the same figure exhibit a positive ΔM step at T_N in the fields of 5 and 6 T, respectively, which is followed by a decay of the magnetization with further increasing temperature. The T_N-related anomalies in the $\rho_{[001]}(T)$ and $M(T)$ curves measured in 6 T exhibit a temperature hysteresis, which is characteristic for a first-order phase transition. In contrast, the T_N-related anomaly in fields up to 5 T show no hysteresis.

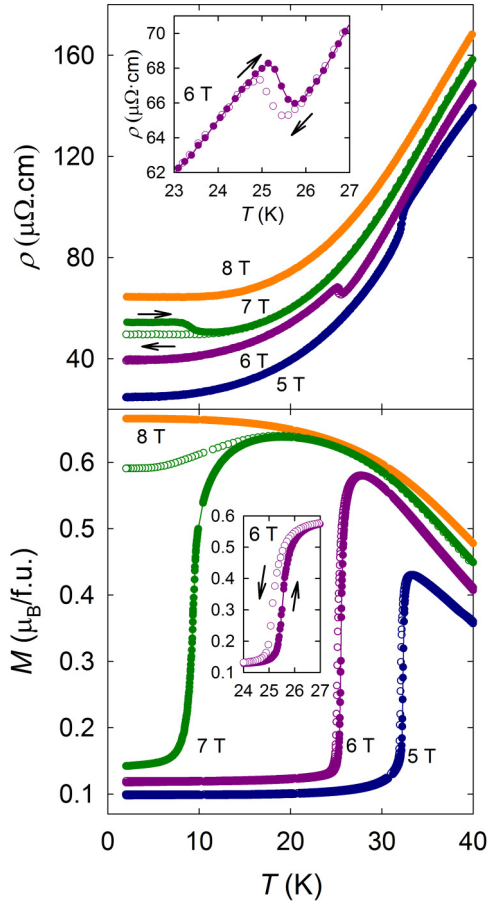

FIG. 4. Temperature dependences of the electrical resistivity $\rho_{[001]}$ (upper panel) and magnetization M (lower panel) of $UIrSi_3$ measured in the magnetic field of 5, 6, 7, and 8 T, respectively, applied in the [001] direction. For 7 T the ZFC (line with open symbols) and FC (line with full symbols) $M(T)$ and $\rho(T)$ curves, respectively, bifurcate below T_N. The $\rho(T)$ curves measured in different fields are mutually shifted by 15 μΩ cm along the vertical axis for clarity. The displayed vertical scale corresponds to the 5-T curve. Inset of lower panel: detail of the hysteresis of the transition in 6 T. The arrows represent the direction of field sweep.

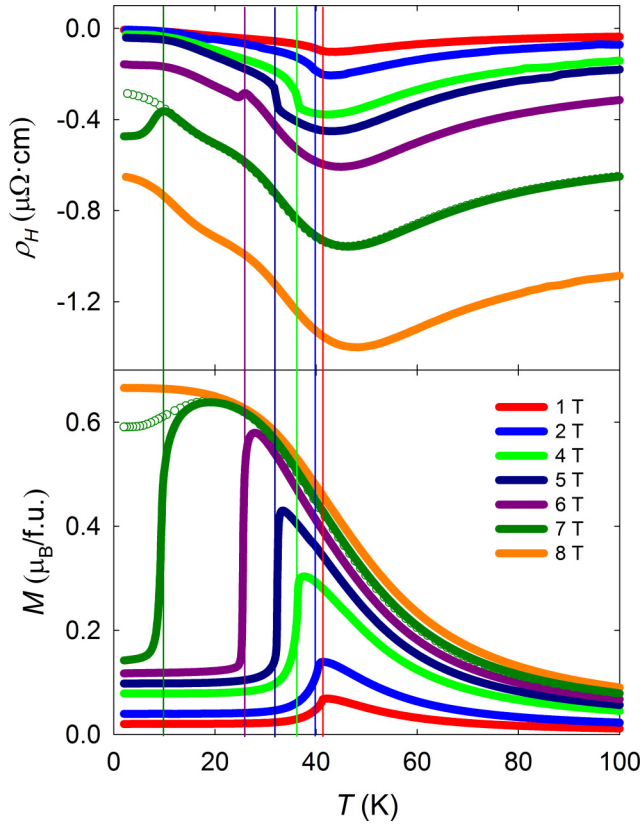

FIG. 5. Temperature dependence of Hall resistivity ρ_H vs T (upper panel) and magnetization M vs T (lower panel) of $UIrSi_3$ in several magnetic fields applied in the [001] direction. The ρ_H vs T and M vs T plots in corresponding magnetic fields are in the same colors. The colored vertical lines represent the T_N values determined by specific-heat measurements. The 7-T vertical line corresponds to the bifurcation point of the ZFC (line with full symbols) and FC (line with open symbols) ρ_H vs T and M vs T curves, respectively. The 6-T, 7-T, and 8-T plots in the upper panel are vertically shifted by −0.1, −0.4, −0.8 μΩ cm, respectively.

The Hall resistivity, ρ_H, in field parallel to [001] is also sensitive to the PM ↔ AFM transition at T_N as can be seen in Fig. 5. The T_N-related anomaly in the $\rho_H(T)$ corresponding to a gradually increasing magnetic field undergoes a development analogous to the normal-resistivity case. It is gradually shifted to lower temperatures to coincide with the T_N-related specific-heat and magnetization anomalies. The Hall resistivity anomaly simultaneously develops with increasing the field from a positive $\partial\rho_H/\partial T$ change in 1 T to a clear negative $\Delta\rho_H$ step in 5 T. T_N coincides with the minimum of $\partial\rho_H/\partial T$ and roughly with the maximum of $\partial M/\partial T$. Also, the Hall resistivity exhibits a contrast between the T_N-related anomalies in fields up to 5 T and those measured in higher fields. In 6 T we suddenly observe a positive $\Delta\rho_H$ step at T_N with temperature hysteresis. The observed qualitative changes of the T_N-related anomalies in the corresponding $M(T)$, $\rho_{[100]}(T)$, $\rho_{[001]}(T)$, and $\rho_H(T)$ dependences in fields between 5 and 6 T may be considered to be connected with the conclusion in Ref. [6], that the change from a SOMPT to a FOMPT happens at a TCP that has been estimated at $\mu_0 H_{tc} \sim 5.8$ T, $T_{tcp} \sim 28$ K.

The ZFC $\rho_H(T)$ curve measured in 7 T also shows a step, which is, however, considerably larger. Similar to normal resistivity and magnetization behavior, the 8-T $\rho_H(T)$ curve is smooth showing no sharp anomaly within the entire temperature range. The 8-T field is sufficiently higher than $\mu_0 H_c$ (7.3 T) at 2 K [6] to entirely destroy the AFM ordering in the ZFC sample and recover the PM state (PPM at sufficiently low temperatures). Application of an 8-T field, when cooling $UIrSi_3$ from high temperatures, prevents any transition to the AFM ordering, i.e., the sample remains PM (PPM at low T). That is why the corresponding 8-T field-cooled (FC) and ZFC $M(T)$, $\rho_{[100]}(T)$, $\rho_{[001]}(T)$, $\rho_H(T)$ curves, respectively, are identical and exhibit no T_N-related anomaly (see Figs. 4 and 5).

The corresponding ZFC and FC $M(T)$, $\rho_{[100]}(T)$, $\rho_{[001]}(T)$, $\rho_H(T)$ curves measured in 7 T bifurcate in the vicinity of T_N (see Figs. 4 and 5). This is reflecting the large field hysteresis of the MT reported in Ref. [6], which

extends around 7 T at low temperatures. When cooling $UIrSi_3$ in 7 T the $M(T)$ values reach a maximum at ∼20 K then decrease by about 10% on further cooling. This indicates that the low-temperature FC state is a somewhat disturbed PPM which, however, exhibits considerably lower resistivity than the low-temperature ZFC state (probably the AFM ground state). The higher resistivity in the AFM state can be also due to the FS truncated by energy gaps caused by a different periodicity of the crystallographic and AFM lattices.

The entire $\rho_H(T)$ dependences measured between 2 and 100 K in fields up to 8 T (see Fig. 5) show a broad valley. The temperature of its minimum roughly coincides with the temperature of the $\partial M/\partial T$ minimum. The ρ_H values are negative, as expected for the ordinary Hall effect in the case of electron conductivity in metals. The positive values in the 8-T and FC 7-T $\rho_H(T)$ dependences at low temperatures reflect large positive contributions due to the AHE in $UIrSi_3$ in the PPM state.

The $\rho_{[100]}(H)$ and $\rho_{[001]}(H)$ data collected at selected temperatures shown in Fig. 6 demonstrate the evolution of MT related resistivity anomalies. In the lower panels, results obtained at $T < T_{tcp}$ at which a FOMPT takes place are displayed. The $\rho_{[001]}(H)$ and $\rho_{[001]}(H)$ curves in the vicinity of H_c qualitatively resemble the corresponding magnetization curves in Ref. [6] taken with negative sign, i.e., the resistivity sharply drops at H_c when sweeping the magnetic field up, and exhibits the asymmetric hysteresis of a MT when sweeping the field down.

The $\rho_{[100]}(H)$, $\rho_{[001]}(H)$ curves in the upper panels of Fig. 6 were measured at temperatures between T_{tcp} and T_N. At these temperatures $UIrSi_3$ undergoes a field-induced SOMPT (AFM↔PM). A dramatic difference in the electrical resistivity response in comparison to the lower-temperature's FOMPT is clearly seen. Here the resistivity considerably increases with increasing field up to the maximum value $\rho(H_c)$. In fields beyond H_c the resistivity values decay fast with increasing H yielding a negative magnetoresistance well above H_c. Contrary to FOMPTs, these transitions have no hysteresis.

The Hall-resistivity isotherms $\rho_H(H)$ measured at temperatures below 28 K show a sudden positive $\Delta\rho_H(H)$ step at H_c and an asymmetric hysteresis, being at lowest temperatures very similar to the magnetization behavior around the FOMPT at H_c [6]. In contrast, the $\rho_H(H)$ curves measured at temperatures higher than 28 K exhibit a slightly rounded negative step at H_c and no field hysteresis. The step gradually smears out with increasing temperature to disappear at temperatures around 40 K. Note that $\Delta\rho_H(H)$ decreases (but does not scale) with the decreasing corresponding $\Delta M(H)$ step.

The observed opposite polarity of the Hall effect step accompanying the FOMPT and the SOMPT, respectively, points to a possible criterion for the determination of the TCP, which separates the FOMPT and SOMPT sections of the magnetic phase diagram.

The main objective of this study is the determination and understanding of the impact of the SOMPT and the FOMPT in $UIrSi_3$ on magnetotransport properties. This would contribute to the usability of magnetotransport as a probe of the types of magnetic phase transitions of antiferromagnets. Closer inspection of $M(T)$,$\rho_{[001]}(T)$, and $\rho_H(T)$ data (see Figs. 4 and 5) measured in the magnetic field parallel to c axis reveals an evolution of magnetization of $UIrSi_3$ with cooling and heating, and the corresponding impact on magnetotransport. When cooling the crystal in a field of 8 T from high temperatures down to 2 K, $UIrSi_3$ is all the time in a paramagnetic state. At 2 K, the highest M and ρ_H values, respectively, are recorded whereas ρ reaches the lowest value. The magnetization is saturated, and so all magnetic moments are aligned (polarized) in the direction of the applied magnetic field, i.e., $UIrSi_3$ is in the PPM regime. The same extreme values of M,$\rho_{[001]}$, and ρ_H, respectively, were measured after cooling the crystal in zero field down to 2 K and subsequently the field was applied and increased up to 8 T (see Fig. 6 in Ref. [6] and Figs. 6 and 7 in this paper). After cooling in zero field to 2 K, $UIrSi_3$ appears in the AFM ground state. When a magnetic field is applied and increasing to 8 T, $UIrSi_3$ undergoes, at H_c, a FOMPT from the AFM to a PM phase with polarized magnetic moments, i.e., the PPM regime. The impact on magnetotransport is in both cases identical; ρ_H reaches a maximum value and ρ approaches a minimum. The positive step of the 2-K magnetization curve, due to the MT at H_c, is accompanied by a positive step of the $\rho_H(H)$ and a negative step of the $\rho(H)$ dependence.

In Figs. 6 and 7 (considering also Fig. 6 in Ref. [6]), we can see that the positive step of the $\rho_H(H)$ and a negative one of the $\rho(H)$ dependence is observed at $T < 28$ K (T_{tcp}) for the transition from an AFM to a PPM, i.e., at which we observe the FOMPT at H_c. Strikingly different $\rho_H(H)$ and $\rho(H)$ behavior is observed at temperatures between T_{tcp} and T_N where $UIrSi_3$ undergoes a SOMPT for the transition from an AFM to a PM state.

We analyzed the Hall resistance data in detail within the scheme based on the empirical formulas (2), (3), (4) following from numerous investigations of the AHE in ferromagnets. In this course we fitted the isofield $\rho_H(T)$ and isothermal $\rho_H(H)$ data series to formulas (S1) and (S2), respectively (see the Supplemental Material [54]) in the context of the available magnetization and electrical resistance data. We have included representative results with descriptions in the Supplemental Material [54].

The individual $\rho_H(T)$ and $\rho_H(H)$ dependences for different fields and temperatures can be reasonably formally fitted to the formulas, however, the variation of fitting parameters does not have to have some physical background. Especially, no reasonable series of fits can be obtained for any chosen constant value of the ordinary Hall-effect coefficient R_0. A possible variation of R_0 in an itinerant $5f$-electron antiferromagnet as $UIrSi_3$ might be due some reorganization of the FS induced in the AFM state by magnetic fields considerably lower than H_c. Relevant band structure calculations may provide results corroborating this idea. In any case the scenario of the Hall effect in $UIrSi_3$ is most probably more complex than that usually investigated using the empirical approach of the AHE applied in the case of ferromagnets. At this stage of understanding we propose the following simple approach to explain the experimental findings. The FOMPTs in $UIrSi_3$ are AFM ↔ PPM transitions, whereas the SOMPTs are AFM ↔ PM, where PM stands for

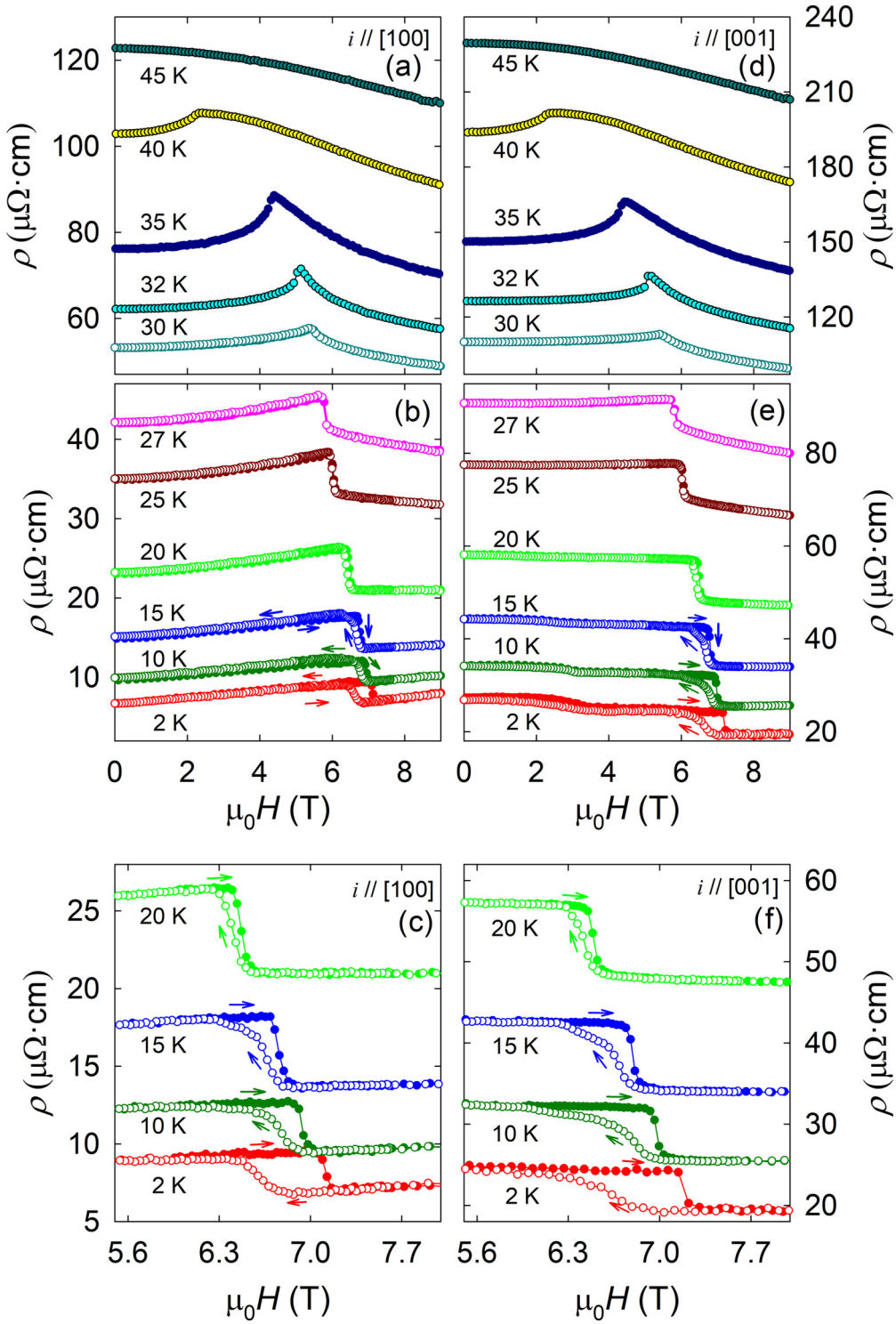

FIG. 6. The electrical resistivity of $UIrSi_3$ at selected temperatures for current parallel to the [100] direction, left panels (a), (b), (c) and the [001] direction, right panels (d), (e), (f) as a function of the magnetic field applied in the [001] direction. The $\rho(H)$ curves in left (right) panels measured at different temperatures are mutually shifted by 2 μΩ cm (6 μΩ cm) along the vertical axis for clarity. The field scale of panels (c) and (f) is expanded to make the evolution of hysteresis at temperatures up to 20 K more visible. The arrows show the direction of field sweep.

a normal paramagnetic state, with normal thermal fluctuations of magnetic moments. The PPM regime at low temperatures, which is characterized by magnetic moments aligned along the field direction, resembles a ferromagnetic state. In the case of full polarization, it yields zero contribution to the electrical resistivity with, on the other hand, a large contribution to anomalous Hall resistivity. The TCP separates the FOMPT and SOMPT regions in the magnetic phase diagram. The relation between the characteristic values of electrical resistance and anomalous Hall resistance of the three states

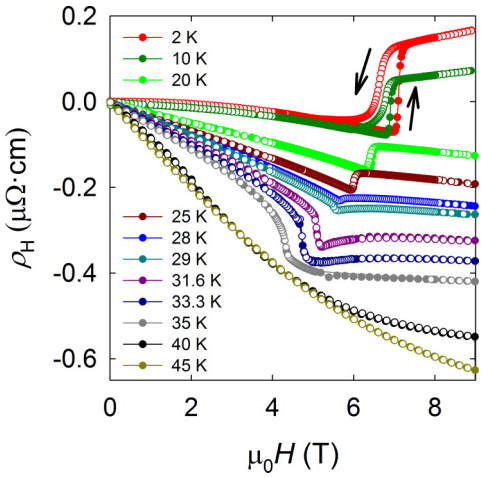

FIG. 7. The Hall resistivity of $UIrSi_3$ at selected temperatures as a function of the magnetic field applied in the [001] direction. Where needed, the arrows show the direction of field sweeps. The hysteresis of the MT at 20 K is 0.25 T, negligible at 25 K and zero at temperatures $\geqslant$28 K.

(regimes) are

$$\rho^{\mathrm{PM}} > \rho^{\mathrm{AFM}} > \rho^{\mathrm{PPM}}, \tag{5}$$

$$\rho_H^{\mathrm{PM}} < \rho_H^{\mathrm{AFM}} < \rho_H^{\mathrm{PPM}}, \tag{6}$$

respectively.

In order to explore the details of the evolution of ρ_{H} and $\rho_{[100]}$ anomalies in the neighborhood of the TCP in the *T*-*H* phase space, we performed thorough measurements of $\rho_{\mathrm{H}}(T)$ and $\rho_{[100]}(T)$ isofield curves for fields 5.2, 5.3, …5.9, 6.0 T and $\rho_{\mathrm{H}}(H)$ and $\rho_{[100]}(H)$ isotherms at temperatures 25, 26, …, 30, 31 K. The results of these measurements are displayed in Figs. S15 and S16 in the Supplemental Material [54]. It is evident that $\Delta\rho_{\mathrm{H}}(T)$ and $\Delta\rho_{\mathrm{H}}(H)$ continually develop from positive to negative values with decreasing magnetic field and increasing temperature, respectively. Considering the estimated values of temperatures and fields for which $\Delta\rho_{\mathrm{H}}(T)$ and $\Delta\rho_{\mathrm{H}}(H)$ values pass through zero we conclude that the change of polarity of jumps of the AHE, as functions of temperature and magnetic field, take place at the TCP.

A closer inspection of isofield $\rho_{[100]}(T)$ and isothermal $\rho_{[100]}(H)$ data reveals that the evolution of electrical resistivity in the neighborhood of the TCP does not correlate with the AHE. A possible explanation may be related to the important role of field-induced spin-flip fluctuations from the AFM state in an enhancement of the electrical resistivity at temperatures above T_{tcp}.

The first-order metamagnetic transitions are characterized by the simultaneous appearance of pronounced jumps in magnetization, specific heat, electrical resistivity, and Hall resistivity. The latter three phenomena are common characteristics of phase transitions involving FS reconstruction, which are called Lifshitz transitions [57]. Specifically considering uranium intermetallic antiferromagnets, recently much interest has been shown in possible Lifshitz transitions in UPt_2Si_2 [58,59]. An interesting case is represented by UPd_2Al_3 in which a cascade of Lifshitz transitions is indicated by anomalies in the Seebeck coefficient in the AFM state in fields lower than H_c, which is followed by a Lifshitz MT at H_c [60].

The Seebeck coefficient

$$S = -\frac{\pi^2 k_B^2}{3|e|} T \left[\frac{\partial ln N(E)}{\partial E} + \frac{\partial ln \tau(E)}{\partial E} \right]_{E=E_F}, \tag{7}$$

where $N(E)$ is the density of states and τ(E) is the relaxation time of conduction electrons [61], is closely connected to characteristics of the FS. An observed sudden change of $S(H)$ provides an indication of a possible change of the energy derivative of the density of states at the Fermi level due to a FS reconstruction connected with the transition.

In Fig. 8, $S(H)$ dependences measured at 15, 20, and 33 K on the $UIrSi_3$ crystal for $\Delta T//c$ are displayed. A clear drop of the value of the Seebeck coefficient at H_c is observed when measured at temperatures below T_{tcp}, at which the first-order AFM↔PPM metamagnetic transition takes place. This result, in conjunction with the observed simultaneous jumps in $\rho(H)$, $\rho_{\mathrm{H}}(H)$, and $C_p(H)$ dependences (for results

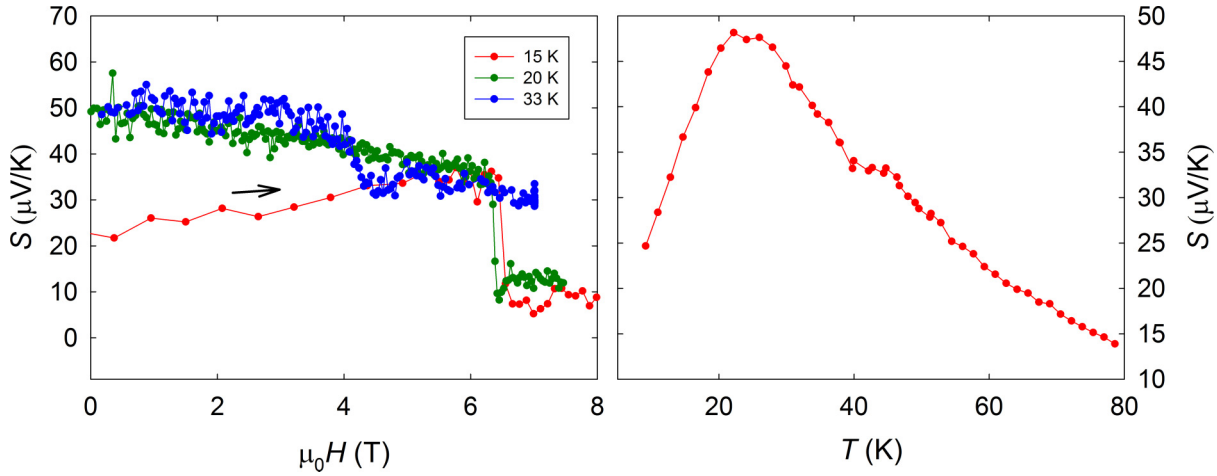

FIG. 8. The Seebeck coefficient of $UIrSi_3$ (left panel) at 15, 20, and 33 K as a function of the magnetic field applied in the [001] direction. The arrow shows the direction of field sweep. Right panel: Temperature dependence in zero magnetic field.

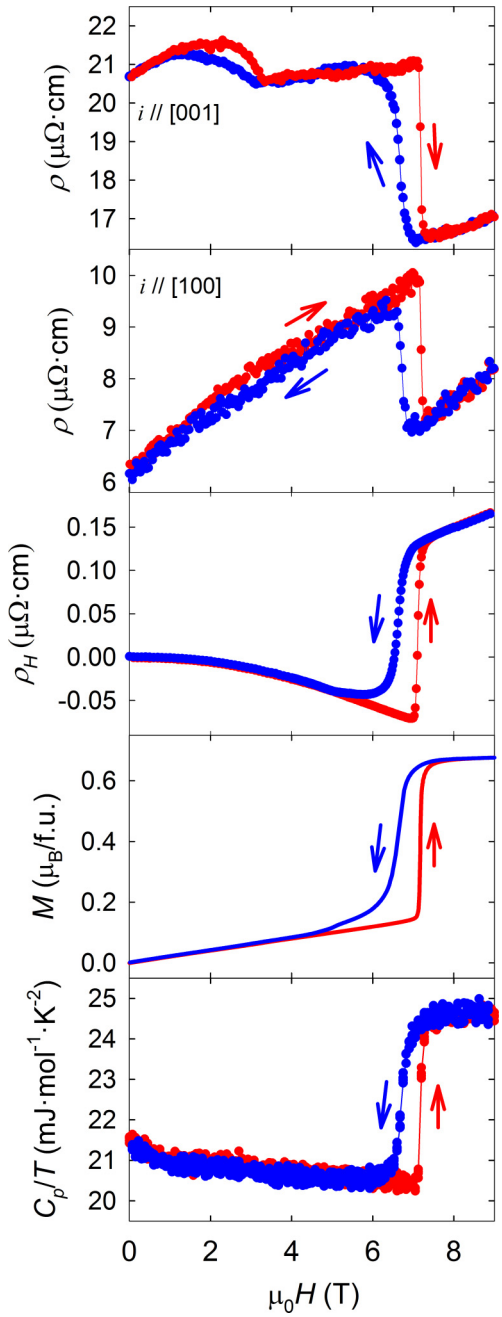

FIG. 9. From top to bottom panel: electrical resistivity for *i*//[001], electrical resistivity for *i*//[100], Hall resistivity, magnetization, and the specific heat divided by temperature of $UIrSi_3$ at 2 K as functions of the magnetic field applied in the [001] direction.

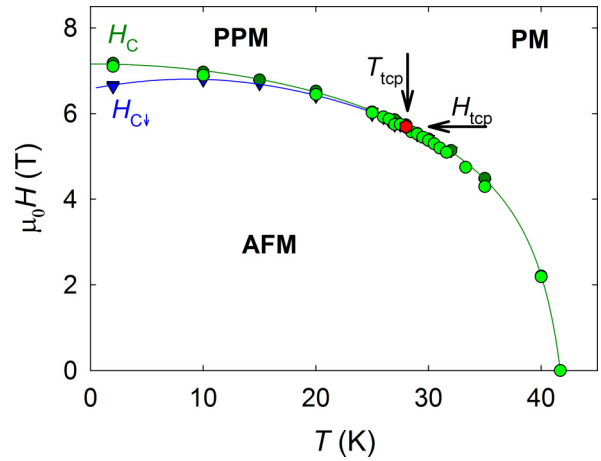

FIG. 10. The magnetic phase diagram of $UIrSi_3$ when the magnetic field is applied along the *c* axis. PM – normal paramagnet, PPM – polarized paramagnet regime as a result of a FOMPT in fields above H_c, AFM – antiferromagnetic phase. H_c and $H_{c\downarrow}$ represented by dark green circles and blue upside-down triangles are defined as inflection points of the field-sweep-up and field-sweep-down $M(H)$, $\rho(H)$, and $\rho_H(H)$ isotherms, respectively, in the vicinity of the MT. The light green circles represent T_N values determined by anomalies on the isofield $C_p(T)$, $\rho(T)$, and $\rho_H(H)$ curves. The red hexagon represents the tricritical point. The lines are guides for the eye.

measured at 2 K, see Fig. 9), suggests that the FOMPT in $UIrSi_3$ is probably a Lifshitz transition, which is characterized by a FS reconstruction. When considering that the uranium $5f$-electron states for $UIrSi_3$ (carrying magnetic moments) are itinerant and can be present at the FS, some FS reconstruction due to the change of magnetic periodicity by the AFM↔PPM transition can be expected. Measurements of x-ray magnetic circular dichroism (XMCD), de Haas–van Alphen (dHvA) and/or the Shubnikov–de Haas (SdH) effect directly testing electronic structure in magnetic fields and relevant band-structure calculations are, however, needed to provide decisive agreement in this issue. On the other hand, no drop at H_c but just a narrow valley has been observed in the $S(H)$ dependence when measured at 33 K ($>T_{tcp}$) as a result of the SOMPT.

The temperature dependence of the Seebeck coefficient as measured at low temperatures and zero magnetic field is shown in Fig. 8 (right panel). It shows a dip at ordering temperature with the presence of the peak centered at $1/2$ T_N, as expected from the gapping of the FS below T_N (see, e.g., Ref. [62]). This leads to a notable difference in the initial slopes for field dependences at 15 K and at higher temperatures.

There is one more feature of $UIrSi_3$, which can be seen from the comparison of the $\rho_{[001]}(H)$, $\rho_{[100]}(H)$, $\rho_H(H)$, $M(H)$, and $C_p(H)$ dependences measured at 2 K as shown in Fig. 9. One can see that the electrical resistivity indicates an additional field-induced bump between 0 and 4 T, which is, however, not reflected in the field dependences of magnetization, Hall resistance, and specific heat, although measured on an identical sample. Assuming a certain analogy with CePtSn [63–65], one can speculate about a transition between two AFM states. Detailed microscopic studies, mainly using neutron scattering and μSR are desired to demonstrate whether the speculation is realistic.

In this context it is worth noting that the magnetic contribution to the electrical resistivity carries some information on the magnetic structure as a result of scattering of conduction electrons from magnetic moments in the material. This is, to a certain extent, comparable to the magnetic scattering of neutrons in magnetic materials. The main difference is that the diffraction of neutron flux from an AFM lattice usually provides different magnetic reflections, carrying rich information on magnetic structure, whereas the scattering of

conduction electrons provides only a different value of electrical resistivity, providing an indication of a possible change of AFM structure. The sensitivity of the electrical resistance to changes in the magnetic structure of U compounds is enhanced by the strong exchange of conducting electrons with moment-carrying U $5f$ electrons, with some states on the FS. In Fig. 10, the magnetic phase diagram of $UIrSi_3$ in the magnetic field applied along the c axis is depicted.

IV. CONCLUSIONS

We have performed a detailed study of the electrical resistance, Hall resistance and thermoelectric power of the Ising noncentrosymmetric antiferromagnet $UIrSi_3$ at various temperatures and magnetic fields with a special emphasis on phenomena associated with magnetic phase transitions between the antiferromagnetic and paramagnetic states. The obtained results demonstrate that the electrical and thermal transport properties can provide valuable information on the character of magnetic phase transformations in antiferromagnets.

We have observed that the unequivocally different character of the FOMPTs and the SOMPTs in $UIrSi_3$ are reflected in the dramatically different transport properties in the neighborhood of the corresponding critical temperatures, T_N, and magnetic fields, H_c. Considering the magnetic parts of electrical resistivity and Hall resistivity, we have suggested a scenario that may successfully explain the observed change of polarity of the $\Delta\rho_H(T)$ and $\Delta\rho_H(H)$ steps at the TCP, which separates the FOMPT and SOMPT segments in the magnetic phase diagram of $UIrSi_3$. Analogous detailed experiments on some other representative Ising-like antiferromagnets are desired to test the universality of the scenario. Neutron-scattering studies of single crystals in magnetic fields are strongly needed in order to confirm the microscopic character of the magnetic regimes assumed in the scenario. Magneto-optic Kerr-effect measurements at various temperatures and magnetic fields would be useful for deeper understanding of the underlying mechanism behind the evolution of the AHE in $UIrSi_3$.

The observed simultaneous appearance of pronounced jumps in the field dependence of specific heat, electrical resistivity, Hall resistivity, and the Seebeck coefficient, respectively, at the FOMPT provide strong indications of a FS reconstruction, which is characteristic of a magnetic-field-induced Lifshitz transition. XMCD, dHvA, and/or SdH experiments in cooperation with relevant band-structure calculations are envisaged in order to get more information on the band structure in magnetic fields and test the idea of a Lifshitz transition in $UIrSi_3$.

ACKNOWLEDGMENTS

This research was supported by the Czech Science Foundation, Grant No. 16–06422S and the Japan Society for the Promotion of Science (JSPS) KAKENHI with Grants No. 15K05156 and No. 15KK0149. Experiments were performed in the Materials Growth and Measurement Laboratory MGML (http://mgml.eu), which is supported by the Ministry of Education, Youth and Sports within the program of Large Research Infrastructures (Grant No. LM2018096). The authors are indebted to Dr. R. Colman for a critical reading and correction of the manuscript.

[1] T. Kasuya, Prog. Rep. Phys. (Kyoto) **22**, 227 (1959).
[2] D. L Mills and P. Lederer, Phys. Chem. Solids **27**, 1805 (1966).
[3] V. Sechovský, L. Havela, K. Prokeš, H. Nakotte, F. R. de Boer, and E. Brück, J. Appl. Phys. **76**, 6913 (1994).
[4] L. Havela, V. Sechovsky, K. Prokes, H. Nakotte, E. Brück, and F. R. de Boer, J. Alloys Compd. **207-208**, 249 (1994).
[5] E. Brück, H. P. Vandermeulen, A. A. Menovsky, F. R. De Boer, P. F. De Châtel, J. J. M. Franse, J. Perenboom, T. Berendschot, H. Van Kempen, L. Havela, and V. Sechovský, J. Magn. Magn. Mater. **104–107**, 17 (1992).
[6] J. Valenta, F. Honda, M. Vališka, P. Opletal, J. Kaštil, M. Míšek, M. Diviš, L. Sandratskii, J. Prchal, and V. Sechovský, Phys. Rev. B **97**, 144423 (2018).
[7] K. Shrestha, D. Antonio, M. Jaime, N. Harrison, D. S. Mast, D. Safarik, T. Durakiewicz, J. C. Griveau, and K. Gofryk, Sci. Rep. **7**, 6642 (2017).
[8] R. L. Stillwell, I. L. Liu, N. Harrison, M. Jaime, J. R. Jeffries, and N. P. Butch, Phys. Rev. B **95**, 014414 (2017).
[9] D. P. Landau, Phys. Rev. Lett. **28**, 449 (1972).
[10] I. S. Jacobs and P. E. Lawrence, Phys. Rev. **164**, 866 (1967).
[11] E. Stryjewski and N. Giordano, Adv. Phys. **26**, 487 (1977).
[12] W. Knafo, R. Settai, D. Braithwaite, S. Kurahashi, D. Aoki, and J. Flouquet, Phys. Rev. B **95**, 014411 (2017).
[13] J. Pospíšil, Y. Haga, Y. Kohama, A. Miyake, S. Kambe, N. Tateiwa, M. Vališka, P. Proschek, J. Prokleška, V. Sechovský, M. Tokunaga, K. Kindo, A. Matsuo, and E. Yamamoto, Phys. Rev. B **98**, 014430 (2018).
[14] E. Brück, H. Nakotte, F. R. de Boer, P. F. de Châtel, H. P. van der Meulen, J. J. M. Franse, A. A. Menovsky, N. H. Kim-Ngan, L. Havela, V. Sechovsky, J. A. A. J. Perenboom, N. C. Tuan, and J. Sebek, Phys. Rev. B **49**, 8852 (1994).
[15] H. Nakotte, E. Brück, F. R. de Boer, A. J. Riemersma, L. Havela, and V. Sechovsky, Physica B **179**, 269 (1992).
[16] G. Binasch, P. Grünberg, F. Saurenbach, and W. Zinn, Phys. Rev. B **39**, 4828(R) (1989).
[17] R. J. Elliott and F. A. Wedgwood, Proc. Phys. Soc. **81**, 846 (1963).
[18] M. N. Baibich, J. M. Broto, A. Fert, F. Nguyen Van Dau, F. Petroff, P. Etienne, G. Creuzet, A. Friederich, and J. Chazelas, Phys. Rev. Lett. **61**, 2472 (1988).
[19] P. M. Levy and S. Zhang, J. Magn. Magn. Mater. **151**, 315 (1995).
[20] H. Yamada and S. Takada, Prog. Theor. Phys. **49**, 1401 (1973).
[21] K. Usami, J. Phys. Soc. Jpn. **45**, 466 (1978).
[22] H. Nozaki and Y. Ishizawa, Phys. Lett. A **63**, 131 (1977).
[23] E. M. Pugh, Phys. Rev. **36**, 1503 (1930).
[24] E. M. Pugh and T. W. Lippert, Phys. Rev. **42**, 709 (1932).
[25] C. M. Hurd, *The Hall Effect in Metals and Alloys* (Plenum, New York, 1972).

[26] L. Berger and G. Bergmann, in *The Hall Effect and its Applications*, edited by C. L. Chien and C. R. Westgate (Plenum, New York, 1980), p. 55 and references therein.
[27] N. Nagaosa, J. Sinova, S. Onoda, A. H. MacDonald, and N. P. Ong, Rev. Mod. Phys. **82**, 1539 (2010).
[28] E. Hall, Philos. Mag. **12**, 157 (1881).
[29] H. Chen, Q. Niu, and A. H. MacDonald, Phys. Rev. Lett. **112**, 017205 (2014).
[30] J. Kübler and C. Felser, EPL **108**, 67001 (2014).
[31] S. Nakatsuji, N. Kiyohara, and T. Higo, Nature (London) **527**, 212 (2015).
[32] C. Sürgers, W. Kittler, T. Wolf, and H. v. Löhneysen, AIP Adv. **6**, 055604 (2016).
[33] L. Šmejkal, Y. Mokrousov, B. Yan, and A. H. MacDonald, Nat. Phys. **14**, 242 (2018).
[34] J. C. Nickerson, R. M. White, K. N. Lee, R. Bachmann, T. H. Geballe, and G. W. Hull, Jr., Phys. Rev. B **3**, 2030 (1971).
[35] J. W. Allen, B. Batlogg, and P. Wachter, Phys. Rev. B **20**, 4807 (1979).
[36] E. Cattaneo, U. Hafner, and D. Wohlleben, in *Valence Instabilities*, edited by P. Wachter and H. Boepart (North-Holland, Amsterdam, (1982), p. 451.
[37] F. G. Aliev, N. B. Brandt, V. V. Moshalkov, and S. M. Chudinov, Solid State Commun. **47**, 693 (1983).
[38] P. Coleman, P. W. Anderson, and T. V. Ramakrishnan, Phys. Rev. Lett. **55**, 414 (1985).
[39] S. Nair, M. Nicklas, J. L. Sarrao, J. D. Thompson, F. Steglich, and S. Wirth, J. Supercond. Nov. Magn. **22**, 201 (2009).
[40] S. Posse, M. S. Wire, and E. Cattaneo, J. Magn. Magn. Mater. **66**, 356 (1987).
[41] A. Fert and P. M. Levy, Phys. Rev. B **36**, 1907 (1987).
[42] M. Van Sprang, R. A. Boer, A. J. Riemersma, L. W. Roeland, A. Menovsky, J. J. M. Franse, and J. Schoenes, J. Magn. Magn. Mater. **76–77**, 229 (1988).
[43] T. Siegrist, M. Olivier, S. P. McAlister, and R. W. Cochrane, Phys. Rev. B **33**, 4370(R) (1986).
[44] J. Schoenes, F. Troisi, E. Brück, and A. A. Menovsky, J. Magn. Magn. Mater. **108**, 40 (1992).
[45] C. Surgers, T. Wolf, P. Adelmann, W. Kittler, G. Fischer, and H. v. Löhneysen, Sci. Rep. **7**, 42982 (2017).
[46] S. M. Thomas, P. F. S. Rosa, S. B. Lee, S. A. Parameswaran, Z. Fisk, and J. Xia, Phys. Rev. B **93**, 075149 (2016).
[47] J. D. Zou, B. G. Shen, J. R. Sun, J. Shen, C. B. Rong, and W. Li, J. Appl. Phys. **103**, 07F301 (2008).
[48] Y. Kobayashi, Y. Aoki, H. Sugawara, H. Sato, V. Sechovsky, L. Havela, K. Prokes, M. Mihalik, and A. Menovsky, Phys. Rev. B **54**, 15330 (1996).
[49] J. R. Jeffries, R. L. Stillwell, S. T. Weir, Y. K. Vohra, and N. P. Butch, Phys. Rev. B **93**, 184406 (2016).
[50] M. A. de Vries, M. Loving, A. P. Mihai, L. H. Lewis, D. Heiman, and C. H. Marrows, New J. Phys. **15**, 013008 (2013).
[51] B. Buffat, B. Chevalier, B. Czeska, J. Etourneau, and P. Hagenmuller, J. Magn. Magn. Mater. **62**, 53 (1986).
[52] Y. Haga, T. Honma, T. Yamamoto, H. Ohkuni, Y. Onuky, M. Ito, and N. Kimura, Jpn. J. Appl. Phys. **37**, 3604 (1998).
[53] J. Pospíšil, K. Prokeš, M. Reehuis, M. Tovar, J. P. Vejpravová, J. Prokleška, and V. Sechovský, J. Phys. Soc. Jpn. **80**, 084709 (2011).
[54] See Supplemental Material at http://link.aps.org/supplemental/10.1103/PhysRevB.100.014401 for a discussion about field-sweeping rate in experiments, conception of metamagnetism in Ising antiferromagnets, additional notes on the polarized paramagnetic regime and crossover to the normal paramagnetic regime, Hall-effect analysis, and detailed evolution of the change of polarity of ρH(T) and ρH(H) at TCP.
[55] N. F. Mott, Proc. R. Soc. A **153**, 699 (1936).
[56] H. Jones, *Handbuch der Physik (Encyclopedia of Physics)* Vol. 19 (Springer, Verlag, Berlin, 1956), p. 266.
[57] I. M. Lifshitz, Zh. Eksp. Teor. Fiz. **38**, 1569 (1960) [Sov. Phys. JETP **11**, 1130 (1960)].
[58] D. Schulze Grachtrup, M. Bleckmann, B. Willenberg, S. Süllow, M. Bartkowiak, Y. Skourski, H. Rakoto, I. Sheikin, and J. A. Mydosh, Phys. Rev. B **85**, 054410 (2012).
[59] D. S. Grachtrup, N. Steinki, S. Sullow, Z. Cakir, G. Zwicknagl, Y. Krupko, I. Sheikin, M. Jaime, and J. A. Mydosh, Phys. Rev. B **95**, 134422 (2017).
[60] A. Gorgout, Ph.D. thesis, Communauté d'universités et d'établissements Université Grenoble Alpes, 2017, https://tel.archives-ouvertes.fr/tel-01563381/document.
[61] R. D. Barnard, *Thermoelectricity in Metals and Alloys* (Taylor, London, 1972).
[62] N. Johannsen, S. Süllow, A. V. Sologubenko, T. Lorenz, and J. A. Mydosh, Phys. Rev. B **78**, 121103(R) (2008).
[63] D. R. Noakes and G. M. Kalvius, Physica B **289–290**, 248 (2000).
[64] B. Janoušová, V. Sechovský, K. Prokeš, and T. Komatsubara, Physica B **328**, 145 (2003).
[65] J. Prokleška, B. Detlefs, V. Sechovský, and M. Míšek, J. Magn. Magn. Mater. **322**, 1120 (2010).